JOURNAL OF AIRCRAFT
Vol. 47, No. 2, March–April 2010

Characterizing Wing Rock with Variations in Size and Configuration of Vertical Tail

Baron Johnson* and Rick Lind†
University of Florida, Gainesville, Florida 32611

DOI: 10.2514/1.45719

Flight at high angle-of-attack conditions, which range beyond wing stall, has numerous advantages for mission performance; however, that flight regime is often affected by adverse behaviors. A particularly notable behavior is associated with uncommanded oscillations primarily about the roll axis and is known as wing rock. This paper investigates wing rock for a small, propeller-powered aerobatic unmanned aerial vehicle with a high degree of vertical symmetry flown at high angle-of-attack conditions. Most importantly, the investigation characterizes the nature of wing rock as a function of size and configuration of the vertical tail. The flight data indicate that wing rock is dependent on the configuration but not on the size of the vertical tail: wing rock oscillations are present for upright but not inverted regardless of vertical tail size. Furthermore, a time-frequency analysis indicates that the wing rock is actually a narrowband phenomenon for which the central frequency varies with time.

I. Introduction

MANY aspects of mission performance are dramatically affected by the angle-of-attack conditions at which an aircraft can operate. In particular, high angle-of-attack conditions in which the aircraft operates beyond wing stall can provide unique characteristics. Such conditions include straight-and-level flight at constant altitude; however, some loss of altitude is also common for various platforms and angle-of-attack conditions. Aircraft typically require a somewhat higher thrust-to-weight ratio, lower wing loading, and larger control surface deflections to perform sustained high angle-of-attack maneuvers as compared to conventional flight requirements.

The significantly reduced airspeed resulting from high angle-of-attack conditions is a primary benefit. Urban operations are especially impacted by airspeed. Low airspeeds can enable sensing missions that want exposure to targets that are in close proximity and thus quickly leave the field of view. Low airspeed coupled with a steep descent can enable maneuvers such as perching, sensor placement, or landing in confined areas without sacrificing ingress and egress speeds [1]. Another beneficial application of high angle-of-attack flight could be for rapid deceleration.

High angle-of-attack flight could also provide greater obstacle avoidance capabilities when flying in urban terrain because the turning radius in high angle-of-attack flight is greatly reduced as compared to that of conventional forward flight. Sensing capabilities could also be enhanced through the use of sensor pointing without the complexity and weight of morphing aircraft or gimbaled sensors [2].

Flight at high angle-of-attack conditions has clear benefits; however, it often exhibits significant wing rock. This phenomenon is described as uncommanded self-induced oscillations primarily about the body-fixed roll axis. Some research has indicated that, although dominated by roll motions, the uncommanded wing rock may actually be a lightly damped dutch roll motion [3–5].

The source of the uncommanded wing rock is not completely known and seems to vary by aircraft configuration. Some research has led to the belief that the wing rock phenomenon is a limit cycle oscillation (LCO) caused either by the loss of dynamic roll damping at high angles-of-attack [6,7] or an aerodynamic hysteresis that generates the springlike forces required to drive the LCO [8–10].

The presence of sideslip has been shown to have an effect on wing rock at high angles-of-attack, both as a cause and mitigator [9,11,12]. Additionally, quite a few studies have found the uncommanded wing rock phenomenon to be somewhat unpredictable, both in magnitude and periodicity [11,13–16].

Some research has determined the phenomenon to be caused by vortices from the leading edges of the wings [3,17,18], whereas other research has determined it to be caused either largely or entirely by vortices generated from slender forebodies impinging upon downstream airframe components such as the vertical tail [15,17,19–23]. Additional research extended these findings to analyze wing rock on a vehicle with and without a vertical tail [24].

The issue of attitude is well known to have an influence on wing rock for aerobatic aircraft in high angle-of-attack flight used by the hobby remote-control (RC) community. In particular, it is well known that many aerobatic aircraft on an RC scale exhibit pronounced wing rock when upright as compared to inverted. Such aircraft are relatively symmetric such that the vertical tail is the main source of geometric difference between upright and inverted. As such, the vertical tail is potentially a significant contributor to wing rock for this class of aircraft. The actual effect of the vertical tail seems to be related to attitude, with upright and inverted having different levels of wing rock along with different values for the coefficient of yaw moment with respect to the angle of sideslip, known as C_{N_β}, and a different interaction of that vertical tail with any vortices shed off the wing or fuselage.

This study investigates the effect of vertical tail size and configuration on wing rock at high angles-of-attack using time- and frequency-domain analysis techniques. The configuration of the

Fig. 1 Mini ShowTime.

Received 29 May 2009; revision received 24 December 2009; accepted for publication 28 December 2009.

*Graduate Student, Department of Mechanical and Aerospace Engineering; vertguy@ufl.edu. Student Member AIAA.

†Associate Professor, Department of Mechanical and Aerospace Engineering; ricklind@ufl.edu. Associate Fellow AIAA.

Table 1 Mini ShowTime specifications

Parameter	Value
Wingspan	1090 mm
Length	1065 mm
Wing area	26.7 dm^2
Flying weight	820 g
Wing loading	30.7–31.8 g/dm^2
Flight speed	0–20 m/s

Table 2 Vertical tail specifications

Tail	Height, mm	Area, cm^2	V_v
Smaller	64.86	90.67	0.01846
Small	90.90	125.22	0.02549
Normal	115.29	162.10	0.03303
Big	140.51	201.70	0.04107
Bigger	165.91	241.73	0.04920

aircraft studied is an unswept tapered wing and conventional horizontal tail, which is a common configuration for aircraft of many sizes. This configuration is potentially subject to several sources of wing rock, including aerodynamic hysteresis and slender forebody vortices impinging on downstream components. The relationship between vertical tail size and configuration and wing rock is examined based on interpreting inertial data from flight testing. The sensors generating such inertial data do not provide sufficient detail about the aerodynamics to fully characterize the flow and, thus, the mechanism causing wing rock; however, the data allow for a parametrization that indicates the effect of the vertical tail on wing rock and provides motivation for further studies using advanced measurements of aerodynamics in a wind tunnel.

This study makes several contributions to the community that supplements previous research. First, it is determined through time-frequency analysis that wing rock with this configuration is a narrow frequency band phenomenon, but with frequency variations in time. Second, wing rock magnitude and frequency do not depend on the size of the vertical tail. Third, wing rock is essentially eliminated when configured with a lower vertical tail of any size due to either the presence of the lower vertical tail or the absence of the upper vertical tail.

These results are achieved by flying both upright and inverted with varying sizes of vertical tail; however, the symmetry of the aircraft, resulting from issues such as lack of geometric dihedral or incidence angles for wings or thrust, eliminates the effect of many contributors that are typically associated with wing rock. As such, the flight parameters, such as angle-of-attack, are identical whether upright or inverted so that the only notable difference is the configuration of the vertical tail.

II. Experimental Testbed

A. Aircraft

The wing rock characteristics of the Mini ShowTime are studied in a high angle-of-attack condition. This electric-powered aircraft, shown in Fig. 1, is a commercially available off-the-shelf platform that is commonly used by the RC community.

This aircraft is constructed from a lightweight balsa wood structure that allows a low wing loading and high thrust-to-weight

Fig. 3 Interchangeable vertical tail mounted on fuselage.

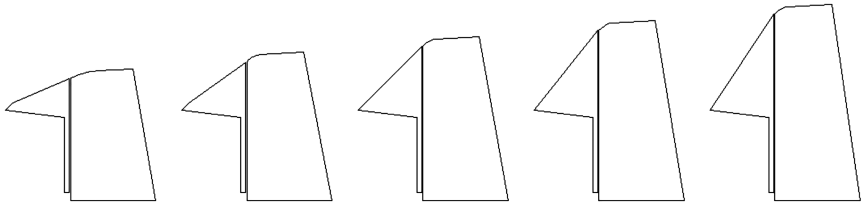

a) b) c) d) e)

Fig. 2 Vertical tails: a) drawing, and b) actual.

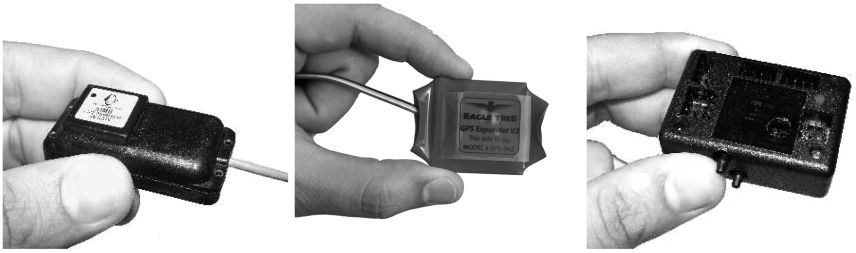

Fig. 4 Airborne sensors: a) IMU, b) GPS receiver, and c) flight data recorder.

ratio. The specific platform has a weight of approximately 820 g along with the characteristics given in Table 1.

This aircraft is used in the community for aerobatics because of its excellent agility and outstanding characteristics at high angle-of-attack conditions. In particular, the aircraft is highly controllable at high angle-of-attack conditions as a result of low wing loading and a high thrust-to-weight ratio along with large control surfaces. These characteristics enable a pilot to maintain orientations within reasonable limits for an extended duration.

The vertical symmetry present on this aircraft makes it ideal for testing the effects of the configuration of the vertical tail. All lifting surfaces are symmetrical and are mounted with zero incidence, and all control surfaces have equivalent deflection in both directions. The wing and horizontal tail have no geometric dihedral and are located along the aircraft centerline, along with the c.g., which results in a similar dihedral effect when upright or inverted except for the contribution from the vertical tail. Thus, a difference in the lateral stability exhibited by the aircraft when upright or inverted is due to the vertical tail placement. The motor is also mounted with zero up/down thrust. Some issues, such as asymmetries due to the canopy or landing gear and propeller effects, likely do not have significant influence on the wing rock. The only notable feature that introduces an asymmetry is the vertical tail, which obviously extends beyond the fuselage in one direction. As such, the platform can generate data that are dominated by effects of the vertical tail.

Also, the vehicle has remarkably similar characteristics with respect to static stability when upright or inverted. It is clearly statically stable in the longitudinal axis in either attitude and remains neutrally stable in the lateral axis. Some variation in directional stability is noted between upright and inverted high angle-of-attack flight, which indicates some probable variation in C_{N_β} that would also alter the wing rock if indeed this behavior is a type of low-damped dutch roll as theorized [3–5].

B. Vertical Tail

The Mini ShowTime aircraft is modified to accommodate interchangeable vertical tails. Vertical tails of varying height are constructed, including the stock tail size and two taller and two shorter vertical tails. The weight difference between vertical tails is negligible in terms of overall weight and c.g. location. The vertical tail volume coefficient is a nondimensional geometric measure of the directional stability of a particular airframe configuration and c.g. location. A vertical tail with a larger area or located farther behind the c.g. typically provides a larger restoring moment due to a sideslip and thus produces a larger vertical tail volume coefficient for a given wing geometry. The vertical tail volume coefficient, V_v, is calculated as follows:

$$V_v = \left(\frac{S_v}{S_w}\right)\left(\frac{L_v}{b}\right) \tag{1}$$

where S_v represents the vertical tail area, L_v represents the distance from the c.g. of the aircraft to the aerodynamic center of the vertical tail, S_w represents the wing area, and b represents the wingspan [25].

The height, area, and vertical tail volume coefficient of each tail are presented in Table 2. The range of tail sizes provides areas and vertical tail volume coefficients ranging from approximately 50 to 150% of the stock tail size. The vertical tails are shown in Fig. 2, and a tail mounted on the modified fuselage is shown in Fig. 3.

The I_{xz} product of inertia of the Mini ShowTime aircraft with the various vertical tails is approximated by treating each component of the airframe and avionics as a point mass. The magnitude of the resulting I_{xz} values range from 5211.5 $\text{g} \cdot \text{cm}^2$ with the smaller tail to 6014.5 $\text{g} \cdot \text{cm}^2$ with the larger tail, which represents a variation of 15%. The sign of this term will be opposite for upright versus inverted flight.

Table 3 Size and mass of avionics

Unit	Size, mm	Mass, g
IMU	$46.5 \times 22.9 \times 13.9$	20
GPS	$36.0 \times 43.0 \times 13.0$	23
FDR	$50.0 \times 35.0 \times 17.0$	22

C. Avionics

An avionics suite is integrated into the aircraft. This suite augments the baseline configuration with sensors that are appropriate for flight testing a vehicle of this size.

Data describing the flight are obtained using the set of instruments shown in Fig. 4. A pair of sensor packages result from an inertial measurement unit (IMU) and the Global Positioning System (GPS). The IMU, which is a MEMSense nIMU, is a MEMS-based unit with temperature compensation and a digital I2C output of three-axis accelerations, angular rates, and magnetic flux. The GPS, which is an Eagle Tree Expander Module, notes the location, groundspeed, course, and Coordinated Universal Time timestamp at a rate of 5 Hz. An additional flight data recorder (FDR), the Eagle Tree Systems FDR Pro, logs the sensor outputs along with barometric altitude and servo commands. This system is able to obtain more than 15 min of data at a rate of 25 Hz.

These sensors are relatively small, as noted in Table 3, and fit easily within the aircraft. The IMU is mounted on a specially installed shelf within the fuselage to lie very close to the center of gravity. The GPS and FDR are installed under the canopy. The sensors increase the mass of the vehicle by approximately 8% and are included on every flight test.

When compared to a high-quality IMU with laser-ring gyros, the nIMU exhibited measurements that yielded attitude and velocity estimates within standard deviations of approximately 0.2 deg on all

Table 4 Technical specifications of IMU

Sensor	Dynamic range	Digital sensitivity	Offset/drift	Noise
Gyro	±600 deg/s	0.01831 deg/s	±1 deg/s	0.56 deg/s
Accelerometer	±5 g	1.5259e − 4 g	±30 mg	4.87 mg
Magnetometer	±1.9 G	5.79e − 5 G	2700 ppm/°C	5.6e − 4 G

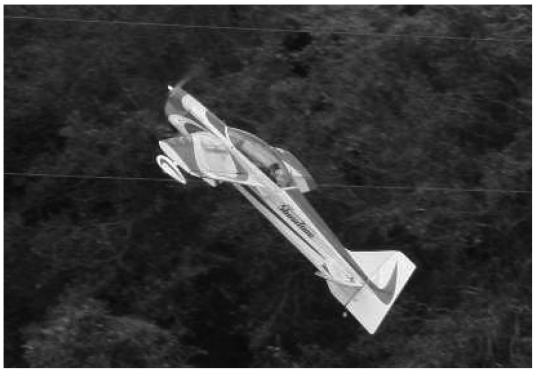

Fig. 5 Mini ShowTime in upright high angle-of-attack flight.

Fig. 6 Mini ShowTime in inverted high angle-of-attack flight.

axes except heading, which exhibited a standard deviation of 0.35 deg [26]. The manufacturer specifications are given in Table 4 for each of the sensors.

III. Flight Testing

Open-loop flight testing was performed to collect data during steady high angle-of-attack flight at a trim condition. Only straight passes were used for data collection to avoid any influences from turning. The passes for data collection were approximately 100 m in length. This length was constrained due to the visual acuity of the pilot and the ability to perform small corrections to maintain the high angle-of-attack flight condition. All flights were performed in a clear field with no obstructions to flight and no turbulence-creating terrain. All flights were performed on a single day with little to no wind at surface level. Any flight maneuvers that were visibly affected by an external disturbance or pilot error were repeated. The altitude for the data collection passes was approximately 30 m. Each flight was limited to no more than 10 min in length due to both the onboard battery supply and the available memory of the FDR.

The pilot attempted to perform all maneuvers at a pitch angle of approximately 45 deg while maintaining level horizontal flight with as few control inputs as possible to maintain such a flight condition. Maintaining level horizontal flight permits the pilot to approximate angle-of-attack as pitch angle, which provides faster and more accurate feedback of the angle of attack than attempting to directly approximate the angle of attack. Also, the pilot performing the flight tests is experienced at performing precision maneuvers from the third-person perspective and has won national titles in both precision and freestyle RC aerobatics. Based on that experience, it is estimated that variations in the angle of attack are less than ± 6 deg within all data sets.

The Mini ShowTime in upright and inverted high angle-of-attack flight is shown in Figs. 5 and 6, respectively.

Flights were performed for each of the ten configurations determined as upright or inverted with each of the five vertical tails. Inverted high angle-of-attack flight was performed in a similar fashion to upright but with trailing-edge-down (positive) elevator deflection to maintain the pitch angle. Additionally, slight differences

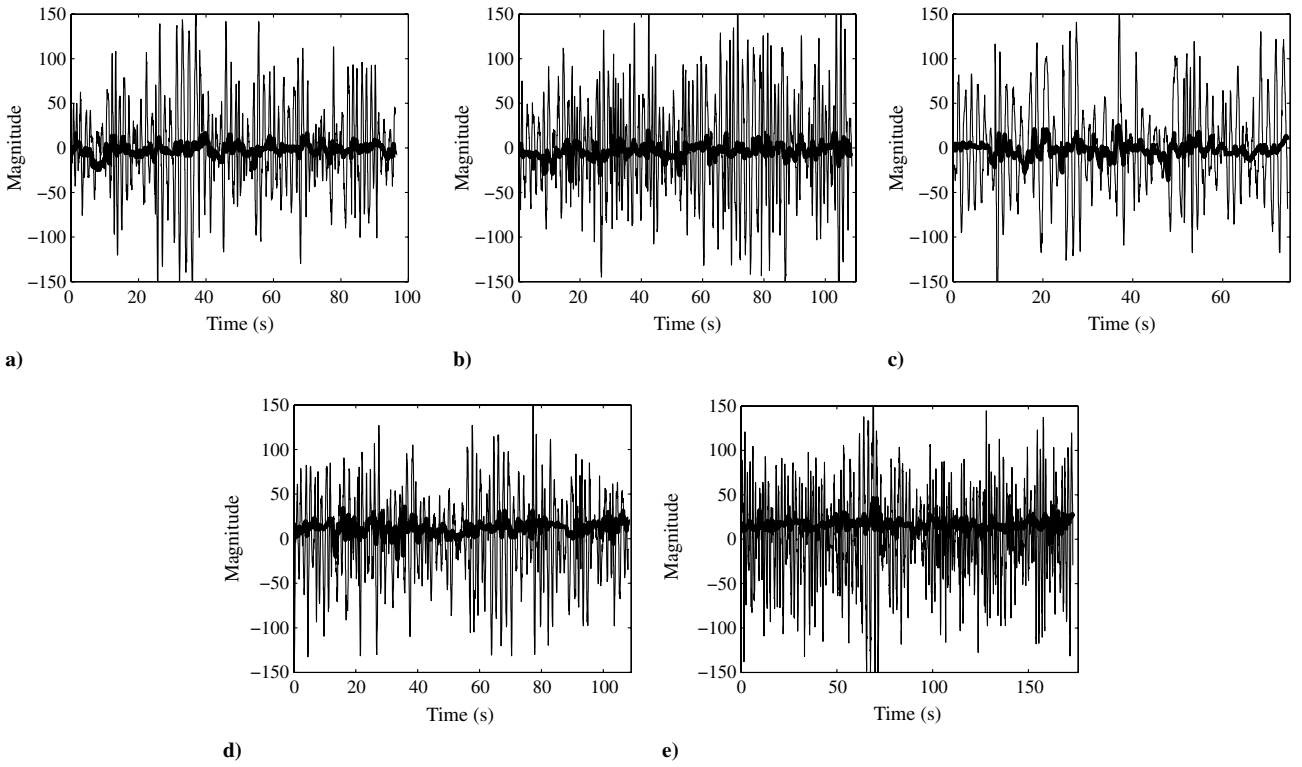

Fig. 7 Time Responses in upright configuration: a) smaller tail, b) small tail, c) normal tail, d) big tail, and e) bigger tail, where the roll rate is denoted with a thin line and the aileron deflection is denoted with a thick line.

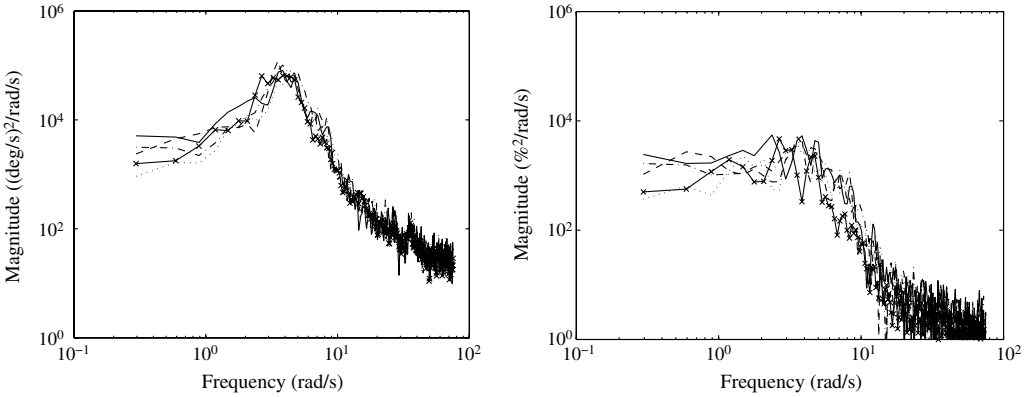

Fig. 8 Power spectral density in upright configuration: a) roll rate, and b) aileron deflection. Smaller tail: dashed line, small tail: dotted-dashed line, normal tail: line, big tail: dotted line, bigger tail: dashed line with x.

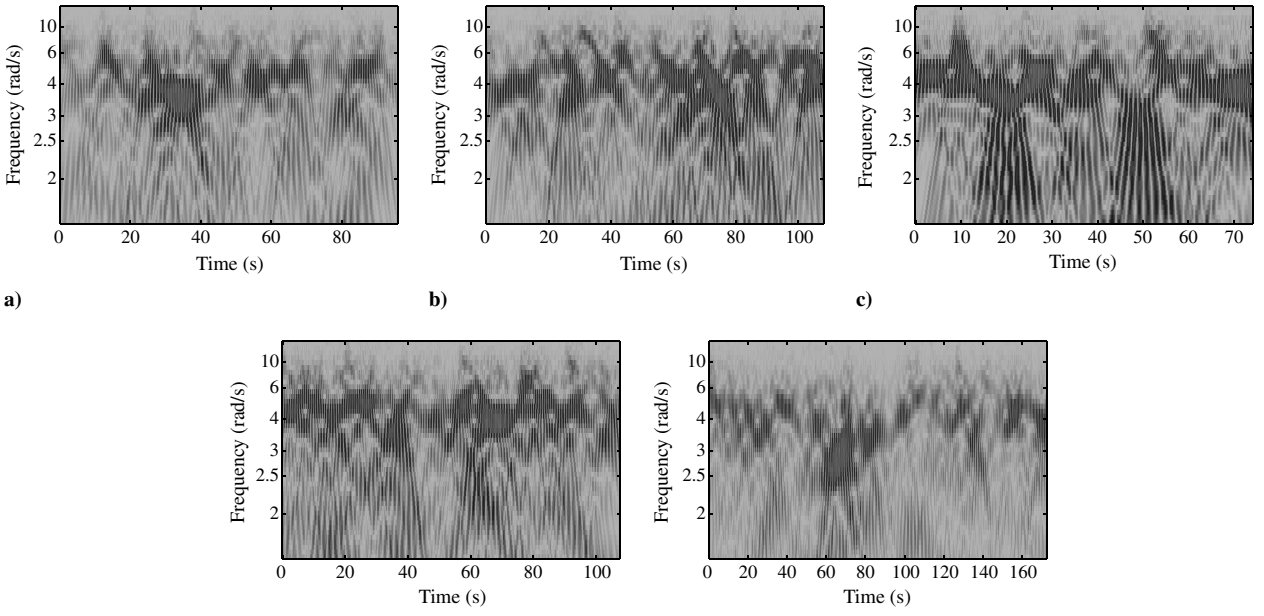

Fig. 9 Wavelet transforms of roll rate in upright configuration: a) smaller tail, b) small tail, c) normal tail, d) big tail, and e) bigger tail.

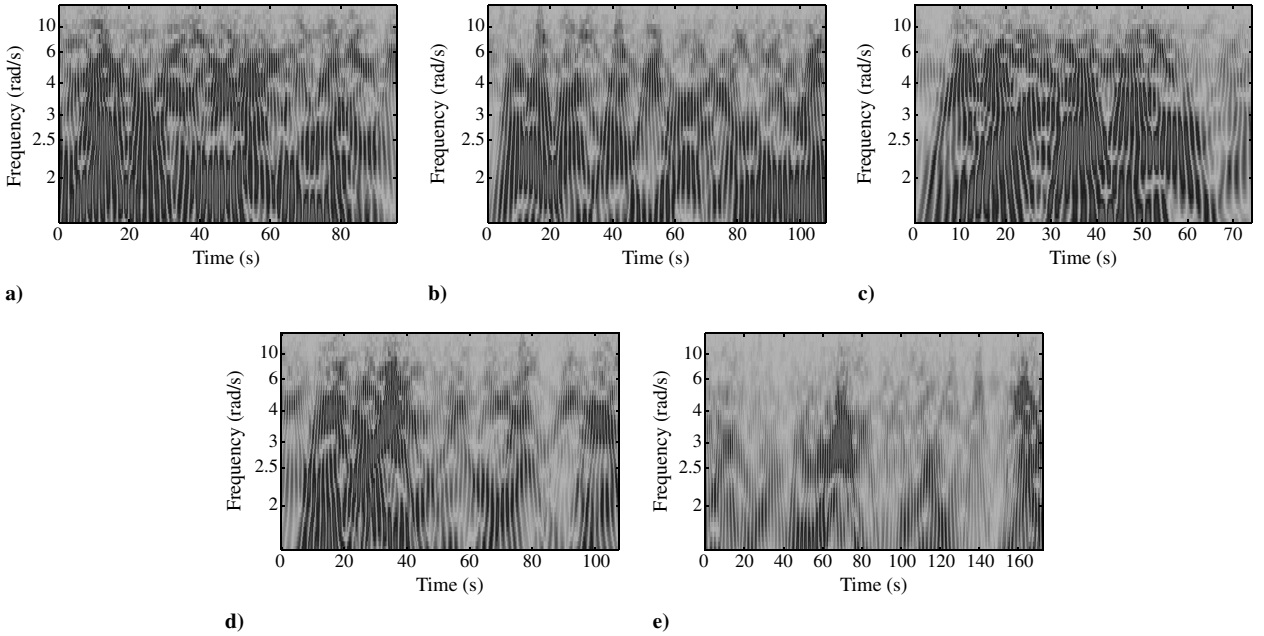

Fig. 10 Wavelet transforms of aileron deflection in upright configuration: a) smaller tail, b) small tail, c) normal tail, d) big tail, and e) bigger tail.

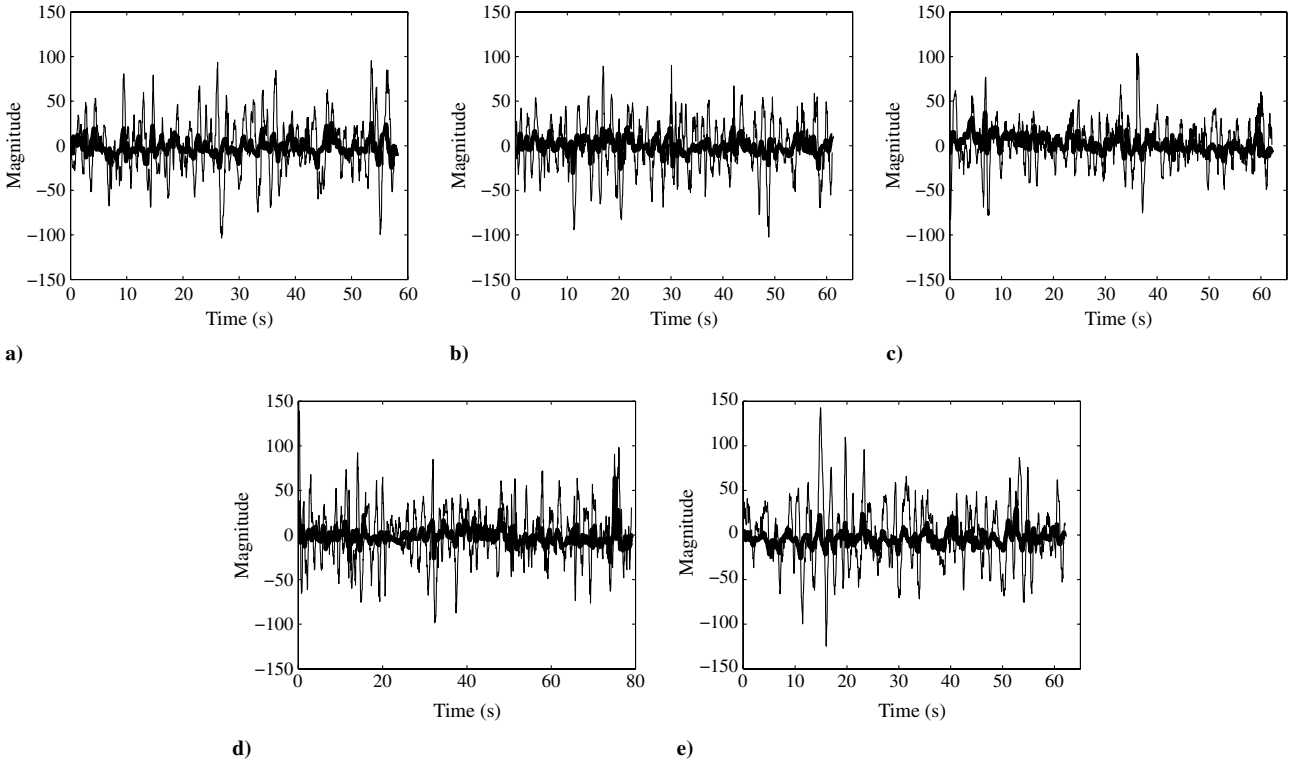

Fig. 11 Time responses in inverted configuration: a) smaller tail, b) small tail, c) normal tail, d) big tail, and e) bigger tail, where the roll rate is denoted with a thin line and the aileron deflection is denoted with a thick line.

in rudder trim existed between upright and inverted due to the large yaw moment from p factor in high angle-of-attack flight. Each flight consisted of establishing the aircraft in either upright or inverted high angle-of-attack flight to determine approximate trim conditions. A minimum of five straight, horizontal passes in high angle-of-attack flight were performed with each tail configuration. An assistant with a stopwatch recorded the times at which each pass began and ended. After each flight, the data from the FDR was downloaded to a computer and the FDR's memory was cleared.

Multiple passes with each tail size were performed and later condensed into individual data sets consisting of all the valid data for each tail and configuration. This approach was taken to create a larger data set to minimize the influence from external disturbances. Additionally, this approach decreases the impact on the analysis results if a single run is performed at a slightly different condition than intended.

IV. Wing Rock

A. Upright Tail

A series of flight tests were performed with the airplane in a standard configuration with the vertical tail pointed upright. The body-axis roll rate measured during these tests is shown in Fig. 7 along with the associated aileron deflections. The aileron deflection is dramatically smaller than the roll rate. Clearly the roll rate shows some amount of periodicity among all the tails; consequently, wing rock appears for any size of these tails. Also, the magnitude of the roll rate shows variation during the response; however, this magnitude is actually somewhat consistent despite variations in the tail size.

The uncertainty in the gyro sensor has minimal influence on the important trends observed in the data. The noise is very small compared to the magnitude of the roll rates. The drift rate has very little impact on the periodic trend, which is analyzed in this study, although it could impact other uses of the sensor such as attitude estimation.

A previous study with the same aircraft and avionics determined a model of the roll rate due to aileron deflection while in the same upright flight condition of an angle of attack of approximately 45 deg. The model was based on aileron doublets of various sizes, found to be fairly linear, and indicated that the lateral dynamics are dominated by a typical mode of roll convergence. This model was then applied to segments of steady high angle-of-attack flight similar to those used in this study to remove the commanded roll rates from the data and extract the uncommanded roll rates.

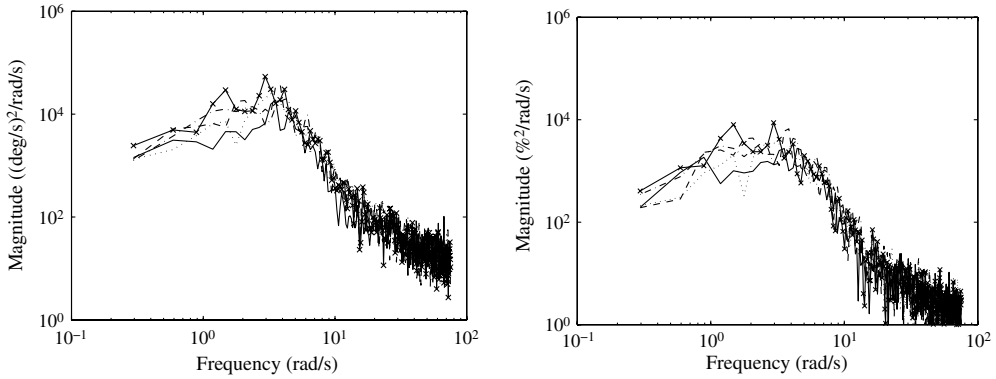

Fig. 12 Power spectral density in inverted configuration: a) roll rate, and b) aileron deflection. Smaller tail: dashed line, small tail: dotted-dashed line, normal tail: line, big tail: dotted line, bigger tail: dashed line with x.

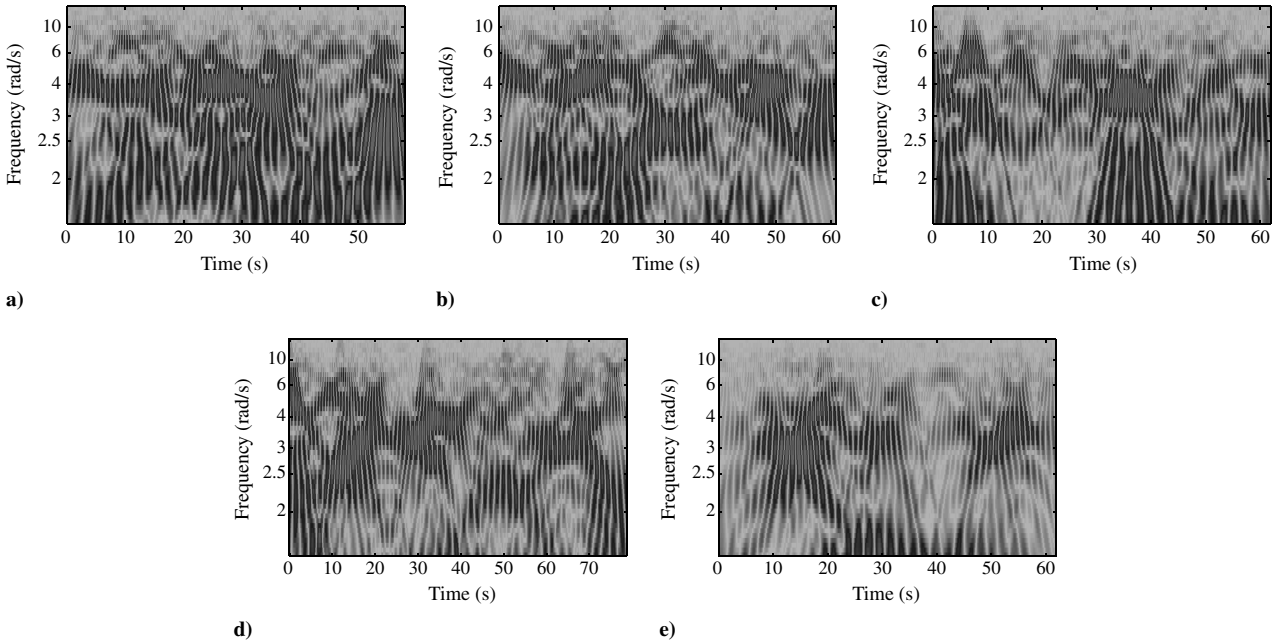

Fig. 13 Wavelet transforms of roll rate in inverted configuration: a) smaller tail, b) small tail, c) normal tail, d) big tail, and e) bigger tail.

Removal of these small commanded roll rates did not significantly alter the frequency content or magnitude of the measured roll rate [27]. Therefore, it can be assumed that the aileron commands in these runs do not significantly alter the nature of the measured roll rate either, as the test flights were performed nearly identically and the data exhibit similar traits.

A frequency-domain representation of the roll rates and aileron deflections from Fig. 7 is computed and shown in Fig. 8 using a power spectral density (PSD). The roll rate shows a consistent amount of energy around 4 rad/s, which correlates to the consistent magnitude observed in the time-domain responses. Also, this peak in energy is actually somewhat broad for every tail and ranges from approximately 2 to 6 rad/s, indicating the wing rock is a broadband phenomenon. The aileron response reflects the self-induced nature of the wing rock because there is no peak in energy introduced by the aileron around 4 rad/s. Rudder deflection is found to be primarily low frequency and indicates no correlation to roll rate near 4 rad/s.

The frequency-domain representations shown in Fig. 8 show that a spike in energy between 2 and 6 rad/s is present in the roll rate but not the aileron deflection for all sizes of tail flown in the upright attitude, indicating that wing rock present in that frequency range is not being induced by the aileron inputs.

A time-frequency representation is computed for the roll rate to investigate the temporal nature of any instantaneous frequencies in the wing rock. These representations are shown in Fig. 9 as computed by wavelet transforms using a Morlet wavelet [28,29]. The lighter shaded regions indicate little-to-no correlation, whereas the darker shaded regions indicate a higher correlation. The wing rock is evident from the high correlations shown around 4 rad/s; however, this representation is notably different than the frequency-domain characterization in Fig. 8. The wing rock is shown to actually have a narrow band of energy when localized in time using Fig. 9. The broadband nature observed in Fig. 8 results from the variations observed in Fig. 9 in the central frequency of that narrow band.

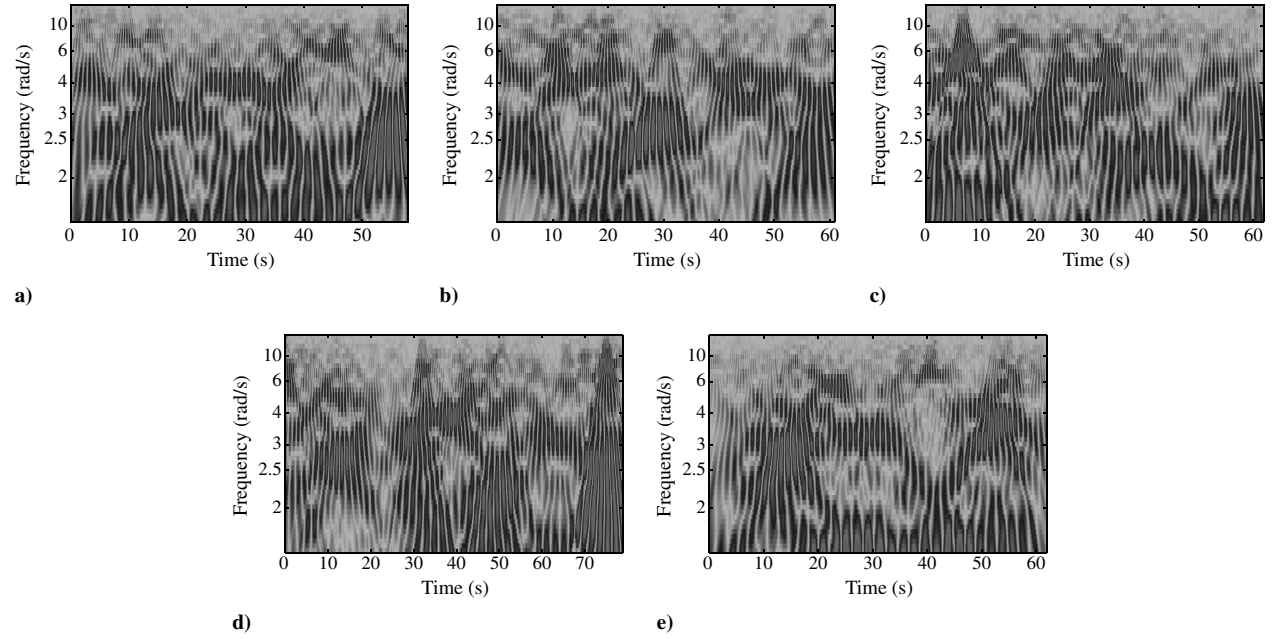

Fig. 14 Wavelet transforms of aileron deflection in inverted configuration: a) smaller tail, b) small tail, c) normal tail, d) big tail, and e) bigger tail.

The wavelet transforms of the aileron deflection, as shown in Fig. 10, do not show significant correlation with the wing rock. Certainly these aileron deflections correlate with the roll rate; however, any correlated energy occurs predominately at lower frequencies than the wing rock. An example of such a correlation is noted in Figs. 9e and 10e between approximately 60 and 75 s at frequencies between about 2.5 and 4 rad/s. This energy is associated with pilot commands and the roll response of the vehicle during standard maneuvering that is not associated with wing rock.

B. Inverted Tail

The airplane was flown in an inverted attitude for each of the different sizes of vertical tail. The roll rate measured during these tests is shown in Fig. 11 along with the associated aileron deflections. The roll rates are approximately an order of magnitude greater than the aileron deflections and both appear to have periodicity. In each case, this magnitude and periodicity are relatively consistent despite variations to the tail.

The frequency-domain representations, shown in Fig. 12, agree with the time-domain analysis of Fig. 11. The roll rate shows a minor broadband peak near 4 rad/s, although it is not as well defined for all sizes of tail as it is in Fig. 8. Also, the peak energy of roll rate in the inverted attitude in Fig. 12 is less than in the upright attitude in Fig. 8. The aileron deflection PSD shows a very similar pattern to that of the upright case, indicating that pilot inputs were similar between the upright and inverted tests. Therefore, differences in roll rate behavior between the upright and inverted tests do not appear to be related to pilot inputs.

A wavelet transform is applied to the time-domain data to generate the time-frequency-domain representation, shown in Fig. 13. Again, the lighter shaded regions indicate little-to-no correlation, whereas the darker shaded regions indicate a higher correlation. These plots show some correlation around 4 rad/s; however, the magnitude of correlation is not excessively high in comparison to the lower frequencies. This lack of excessive correlation agrees with the PSDs in Fig. 12 and is evident for each tail.

A similar time-frequency representation of the aileron data, as computed through wavelet transform and shown in Fig. 14, indicates a strong correlation to the roll rates that are shown in Fig. 13. In particular, most of the peaks in correlation for roll rate are matched by a peak in aileron at the same time and frequency.

C. Parametrization

The nature of wing rock is parameterized with the size and configuration of the vertical tail. In this case, the frequencies and peak magnitudes of the associated oscillations are extracted from the time histories in Figs. 7 and 11. The frequencies and peak magnitudes are then averaged to generate the data in Fig. 15. These data demonstrate that the magnitude of wing rock appears to depend solely on the attitude of the vertical tail and not the size of the vertical tail. This magnitude for any size of vertical tail when upright is nearly double that of the magnitude for any size of vertical tail when inverted. Futhermore, the frequency of wing rock is nearly identical for any size and attitude of the vertical tail.

The difference in magnitude of wing rock between upright and inverted flight is likely more pronounced than Fig. 15 indicates. Figures 9 and 10 show little correlation between aileron input and roll rate frequencies in the upright configuration; however, Figs. 13 and 14 indicate that a strong correlation exists between roll rate and aileron input frequencies at essentially all times when roll rate oscillations are observed in the inverted configuration. This correlation indicates that wing rock is either virtually nonexistent or at least significantly more controllable when in the inverted configuration, so that high angle-of-attack flight for this vehicle is not adversely affected by wing rock when inverted.

The upper and lower bounds on frequency for uncommanded wing rock are extracted from Figs. 8 and 9 and are shown in Fig. 16. Only uncommanded motion associated with wing rock is of interest. Hence, there are no data for the inverted portion of Fig. 16 because there appears to be no uncommanded roll oscillations. The upper and

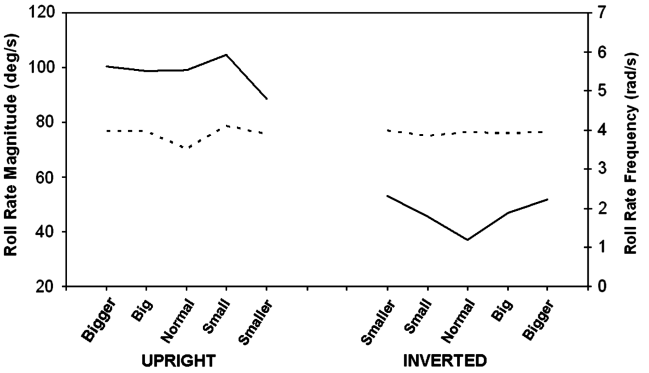

Fig. 15 Mean roll rate peak magnitudes (line) and peak-to-peak frequencies (dotted line).

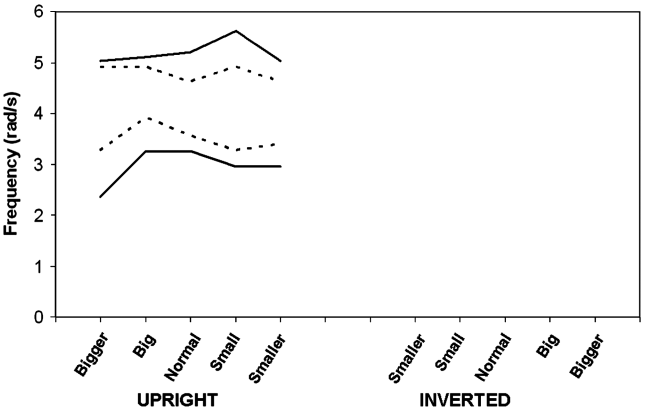

Fig. 16 Upper and lower bounds of uncommanded wing rock frequency from PSDs (line) and wavelets (dotted line).

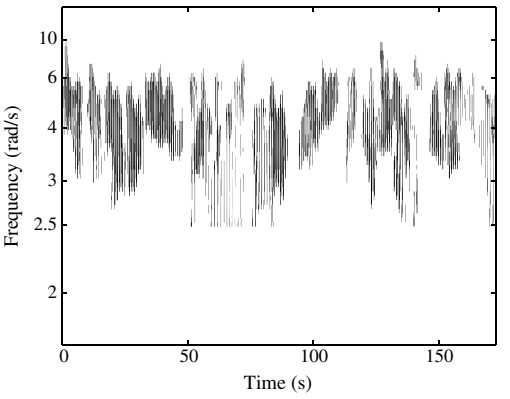

Fig. 17 Filtered wavelet transform of roll rate with upright bigger tail.

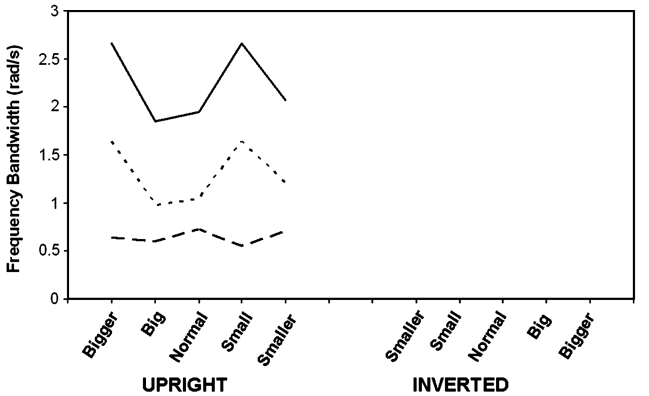

Fig. 18 Average uncommanded wing rock bandwidth: bounds from PSDs (line) and wavelets (dotted line), and localized from wavelets (dashed line).

lower bounds as determined by both the PSDs and wavelets are fairly consistent for all tail sizes. These bounds indicate that wing rock exists across a spectrum of frequencies with bandwidths of approximately 2 rad/s for all tail sizes.

The time-frequency representations shown in Fig. 9 actually indicate that the wing rock oscillation is much narrower in bandwidth when localized in time than Fig. 16 indicates. The wavelet plots of Fig. 9 were filtered to provide a measure of the true bandwidth localized in time. Correlation below a threshold was set to zero on the plot for the purpose of clarifying the region of interest. Additionally, high correlation in aileron input was filtered out of the correlation of the roll rate to isolate uncommanded wing rock. An example of a filtered wavelet plot is shown in Fig. 17 for the bigger tail in upright configuration.

The average bandwidth of the localized time-frequency information from the filtered wavelet plots for each vertical tail is extracted and shown in Fig. 18 along with the bandwidth associated with the bounds from Fig. 16. Again, only uncommanded wing rock is of interest, and so only the upright configuration is used in Fig. 18. The average bandwidth at localized points in time is notably smaller than the bounds as indicated by both the PSDs and wavelets shown in Fig. 16. Such a discrepancy indicates that wing rock is actually a fairly narrowband phenomenon for which the central frequency varies with time. As such, a traditional frequency-domain analysis indicates a broadband behavior by noting the bounds, whereas a time-frequency analysis indicates the narrowband behavior by noting the localized properties at instantaneous times. The cause of such variation in frequency with time is unknown; however, some amount of variation would be expected if the underlying dynamics associated with wing rock are indeed nonlinear, so that any response depends on the phase-plane characteristics along with the initial conditions for the LCO [6–10].

V. Conclusions

Uncommanded wing rock at high angle-of-attack flight is a complex phenomenon. An extensive set of high angle-of-attack flight data from a remote-controlled aircraft with multiple vertical tail sizes and configurations is analyzed. The aircraft has very few asymmetries, except for the vertical tail, which allows upright and inverted flight to be compared to analyze the influence of the vertical tail. Time-frequency analysis indicates that, when the vertical tail is in the upright position, pronounced uncommanded wing rock is present at approximately 4 rad/s for all sizes of vertical tail. Uncommanded wing rock was virtually eliminated in the inverted attitude with a vertical tail of any size. These findings indicate that for this aircraft uncommanded wing rock is greatly influenced by the presence or absence of upright and inverted vertical tails, but not necessarily the size, area, or volume of such vertical tails within the range tested in this study. This result suggests that none of the varied parameters impact the wing rock behavior individually, as it is unlikely that they produce perfectly countering trends.

A potential implication for aircraft design is that either the presence of a lower vertical tail or the absence of an upper vertical tail may help mitigate the undesirable characteristic of uncommanded wing rock at high angles of attack. However, this study examines a single aircraft with a particularly convenient configuration. The broad applicability of these results to aircraft of different configurations and sizes is unknown.

Additionally, time-frequency analysis through wavelet transforms indicates that the wing rock is a narrowband phenomenon that is bounded by a broader band, and not a broadband phenomenon as traditional frequency-domain analysis indicates.

Acknowledgments

This work was supported jointly by the U.S. Air Force Research Laboratory and the U.S. Air Force Office of Scientific Research under F49620-03-1-0381 and F49620-03-1-0170, along with a fellowship provided by the Alumni Fellows Program at the University of Florida.

References

[1] Wright, K., and Lind, R., "Sensor Emplacement on Vertical Surfaces for a Biologically Inspired Morphing from Bats," *Journal of Aircraft*, Vol. 46, No. 4, 2009, pp. 1450–1454. doi:10.2514/1.42859

[2] Grant, D., Abdulrahim, M., and Lind, R., "Flight Dynamics of a Morphing Aircraft Utilizing Multiple-Joint Wing Sweep," AIAA Paper 2006-6505, 2006.

[3] Hwang, C., and Pi, W. S., "Some Observations on the Mechanism of Aircraft Wing Rock," *Journal of Aircraft*, Vol. 16, No. 6, June 1979, pp. 366–373. doi:10.2514/3.58533

[4] Liebst, B., and Nolan, R., "Method for the Prediction of the Onset of Wing Rock," *Journal of Aircraft*, Vol. 31, No. 6, November 1994, pp. 1419–1421. doi:10.2514/3.46669

[5] Regenie, V., Gatlin, D., Kempel, R., and Matheny, N., "The F-18 High Alpha Research Vehicle: A High-Angle-of-Attack Testbed Aircraft," NASA TM 104253, Dryden Flight Research Facility, Edwards, CA, Sept. 1992.

[6] Go, T. H., "An Analytical Approach to the Aircraft Wing Rock Dynamics," AIAA Paper 2001-4426, Aug. 2001.

[7] Go, T. H., and Ramnath, R. V., "An Analysis of the Two Degree-of-Freedom Wing Rock on advanced Aircraft," *Journal of Guidance, Control, and Dynamics*, Vol. 25, No. 2, March–April 2002, pp. 324–333. doi:10.2514/2.4885

[8] Schmidt, L. V., "Wing Rock Due to Aerodynamic Hysteresis," *Journal of Aircraft*, Vol. 16, No. 3, March 1979, pp. 129–133. doi:10.2514/3.58495

[9] Lie, F. A. P., and Go, T. H., "Analysis of Single Degree-of-Freedom Wing Rock due to Aerodynamic Hysteresis," AIAA Paper 2007-6489, 2007.

[10] Abramov, N., Goman, M., Demenkov, M., and Khabrov, A., "Lateral-Directional Aircraft Dynamics at High Incidence Flight with Account of Unsteady Aerodynamic Effects," AIAA Paper 2005-6331, 2005.

[11] Bauer, J., Clarke, R., and Burken, J., "Flight Test of the X-29A at High Angle-of-Attack: Flight Dynamics and Controls," NASA TP 3537, Dryden Flight Research Center, Edwards, CA, Feb. 1995.

[12] Liebst, B. S., and DeWitt, B. R., "Wing Rock Suppression in the F-15 Aircraft," AIAA Paper 1997-3719, 1997.

[13] Iliff, K. W., and Wang, K. C., "X-29A Lateral-Directional Stability and Control Derivatives Extracted from High-Angle-of-Attack Flight Data," NASA TP 3664, Dryden Flight Research Center, Edwards, CA, Dec. 1996.

[14] Davison, M. T., "An Examination of Wing Rock for the F-15," U.S. Air Force Inst. of Technology AFIT/GAE/ENY/92M-01, Wright–Patterson Air Force Base, Dayton, OH, Feb. 1992.

[15] Brandon, J. M., and Nguyen, L. T., "Experimental Study of Effects of Forebody Geometry on High Angle-of-Attack Stability," *Journal of Aircraft*, Vol. 25, No. 7, July 1988, pp. 591–597. doi:10.2514/3.45628

[16] Meyer, R. R., "Overview of the NASA Dryden Flight Research Facility Aeronautical Flight Projects," NASA TM 104254, Dryden Flight Research Facility, Edwards, CA, Aug. 1992.

[17] Ericsson, L. E., "Various Sources of Wing Rock," *Journal of Aircraft*, Vol. 27, No. 6, June 1990, pp. 488–494. doi:10.2514/3.25309

[18] Walton, J., and Katz, J., "Application of Leading-Edge Vortex Manipulations to Reduce Wing Rock Amplitudes," *Journal of Aircraft*, Vol. 30, No. 4, July–Aug. 1993, pp. 555–557. doi:10.2514/3.46381

[19] Ericcson, L. E., "Sources of High Alpha Vortex Asymmetry at Zero Sideslip," *Journal of Aircraft*, Vol. 29, No. 6, Nov.–Dec. 1992, pp. 1086–1090. doi:10.2514/3.56864

[20] Ericsson, L. E., "Wing Rock Generated by Forebody Vortices," *Journal of Aircraft*, Vol. 26, No. 2, Feb. 1989, pp. 110–116. doi:10.2514/3.45731

[21] Ericsson, L. E., "Further Analysis of Wing Rock Generated by Forebody Vortices," *Journal of Aircraft*, Vol. 26, No. 12, Dec. 1989, pp. 1098–1104. doi:10.2514/3.45886

[22] Ericsson, L. E., "Effect of Deep-Stall Dynamics on Forebody-Induced Wing Rock," AIAA Paper 1996-3404, 1996.

[23] Alcorn, C. W., Croom, M. A., Francis, M. S., and Ross, H., "The X-31 Aircraft: Advances in Aircraft Agility and Performance," *Progress in Aerospace Sciences*, Vol. 32, 1996, pp. 377–413.

doi:10.1016/0376-0421(95)00006-2

[24] Gilbert, W. P., Nguyen, L. T., and Gera, J., "Control Research in the NASA High-Alpha Technology Program," *AGARD Fluid Dynamics Panel Symposium on Aerodynamics of Combat Aircraft Control and Ground Effects*, CP-465, AGARD, Neuilly-sur-Seine, France, Oct. 1989.

[25] Smith, H. C., *The Illustrated Guide to Aerodynamics*, TAB Books, Blue Ridge Summit, PA, 1992, pp. 228–229.

[26] Perry, J., Mohamed, A., Johnson, B., and Lind, R., "Estimating Angle of Attack and Sideslip Under High Dynamics on Small UAVs," *Proceedings of the 21st International Technical Meeting of the Satellite Division of the Institute of Navigation*, Institute of Navigation, Manassas, VA, Sept. 2008, pp. 1165–1173.

[27] Johnson, B., and Lind, R., "High Angle-of-Attack Flight Dynamics of Small UAVs," AIAA Paper 2009-61, 2009.

[28] Strang, G., and Nguyen, T., *Wavelets and Filter Banks*, Wellesley–Cambridge Press, Wellesley, MA, 1996, Chap. 1.

[29] Misiti, M., Misiti, Y., Oppenheim, G., and Poggi, J., *Wavelet Toolbox User's Guide, Version 2*, The MathWorks, Inc., Natick, MA, 2000, Chap. 1, 6.